Energy 36 (2011) 4048–4054

Contents lists available at ScienceDirect

Energy

journal homepage: www.elsevier.com/locate/energy

Investigation into topping cycle: Thermal efficiency with and without presence of thermoelectric generator

A.Z. Sahin*, B.S. Yilbas, S.Z. Shuja, O. Momin

Mechanical Engineering Department, King Fahd University of Petroleum and Minerals, Dhahran, Saudi Arabia

ARTICLE INFO

Article history:
Received 7 December 2010
Received in revised form
17 April 2011
Accepted 26 April 2011
Available online 23 May 2011

Keywords:
Thermoelectric
Topping cycle
Solar
Heating

ABSTRACT

Thermoelectric power generation due to solar heating is a current interest in green energy research. One of the applications of the thermoelectric power generator is involved with the topping cycle, in which the thermoelectric generators were placed on the heat collector elements of a conventional solar concentration power plant. Although the topping cycle is practical and easy to operate, the efficiency of the thermal system with and without thermoelectric generator needs to be examined. In the present study, thermal efficiency of the topping cycle is analyzed and compared with its counterpart without the presence of the thermoelectric elements. Thermodynamic analysis for the efficiency of both the systems with and without thermoelectric generator is presented. The fluid flow and heat transfer in a tube with presence of thermoelectric elements resembling the solar heating system incorporated in the topping cycle are simulated numerically. It is found that, for a certain combination of operating and thermoelectric device parameters, thermal efficiency of the topping cycle becomes slightly higher than that of the same system without the presence of the thermoelectric generators.

1. Introduction

Thermoelectric power generation is one of the current interests in clean energy research in view of the recycling of wasted heat. Due to the fact that abundant waste of heat is involved with solar driven power plants, thermoelectric power generation becomes an attractive application with solar driven power plants. Thermoelectric power generation technology has been widely used for many years in DC power generation, heating and cooling applications. Although recent developments in nanotechnology have helped to improve the efficiency of the thermoelectric generators, they are not yet competitive with other electrical energy generation technologies from the efficiency perspective. Thermoelectric efficiency of these generators has generally been limited to about 5–6% [1]. However, they are easy to operate, compact, longer-lived, and require low maintenance cost. In solar thermal power plants the thermoelectric devices can utilize the waste heat to generate electricity; thus, the efficiency of the solar thermal power plant can be improved. Thermoelectric devices are friendly to the environment, so they have attracted increasing attention as a green and flexible source of electricity.

Improvement of thermoelectric generator performance has been the objective of many of investigations. Kassas [2] carried out thermodynamic analysis of a thermoelectric device. He considered the thermoelectric diode and calculated the electronic as well as the Carnot efficiency of the device. He found that increasing emitter temperature increases the Carnot efficiency of the thermoelectric device. He also found that the second law efficiency increases with emitter to collector temperature ratio and reduces with increasing collector temperature as a result of the increase in collector current flow. Yamashito [3] derived some thermal rate equations by considering the temperature dependencies of the electrical resistivity and thermal conductivity of the thermoelectric materials into the thermal rate equations. He derived the energy conversion efficiencies from both the new and conventional thermal rate equations and discussed the effect of the temperature dependency of the properties. He concluded that the temperature dependence of the electrical resistivity and thermal conductivity significantly influences the efficiency of the thermoelectric generator. Performance of thermoelectric devices was also studied by Yilbas and Sahin [4]. They formulated the optimum values of the slenderness ratio and external load parameter for maximizing the device efficiency. They found that for a fixed thermal conductivity ratio, the external load parameter increases with increasing the slenderness ratio while the electrical conductivity ratio of the *p* and *n* pins in the device reduces.

* Corresponding author. Tel.: +966 3 860 2548; fax: +966 3 860 2949.
E-mail address: azsahin@kfupm.edu.sa (A.Z. Sahin).

0360-5442/$ – see front matter © 2011 Elsevier Ltd. All rights reserved.
doi:10.1016/j.energy.2011.04.044

Hsiao et al. [5] studied the development of thermoelectric generators for implementation in the internal combustion engine. They found that installing the thermoelectric generators on the exhaust pipe would yield better results that installing them on the radiator. Champier et al. [6] studied the feasibility of using thermoelectric module in a biomass cook stove for generating electricity to power the fan and give light. They discussed the feasibility of adding commercial thermoelectric modules to the biomass cook stove to come up with the best position of the modules.

Design optimization for the thermoelectric generators has been subject of some previous investigations. Kubo et al. [7] carried out experimental and numerical investigation on the performance of thermoelectric device and studied the relationship between electrical power, conversion efficiency, and incision size and the cold-side temperature. They found that the electrical power generated, the conversion efficiency, and the incision size depend on the cold-side temperature. Guo et al. [8] studied the design performance of a low-temperature waste heat thermoelectric generator both analytically and experimentally. They found that expanding heat sink surface area in a proper range and enhancing cold-side heat transfer capacity can enhance the performance. Omer and Infield [9] investigated the geometrical optimization of the thermoelectric elements. The model considers the effect of the parameters that contribute to the heat transfer process associated with the thermoelectric devices in power generation mode. Their optimization of the element length was based on maximum power output from the device, rather than efficiency.

Utilization of thermoelectric devices for cooling and refrigeration has been studied extensively. Astrian et al. [10] studied the improvement of the coefficient of performance in the thermoelectric refrigeration by the optimization of heat dissipation. They showed that the use of thermosyphon with phase change increases the coefficient of performance up to 32%. Performance optimization of thermoelectric refrigeration was also subject of the investigations by Khattab and Shenawy [11]. They showed that five thermocouples of the thermoelectric generator can drive one thermocouple of the thermoelectric cooler. Later Abdul-Wahab et al. [12] studied the design of portable solar thermoelectric refrigerator experimentally. They showed that the temperature of the refrigeration could be reduced from 27 °C to 5 °C in approximately 44 min with a coefficient of performance of about 0.16.

A common use of thermoelectric devices is cooling of electronic devices. Many researchers have contributed in the investigation for different aspects of thermoelectric cooling of electronic devices. Hwang et al. [13] analyzed the planar multistage micro thermoelectric cooler for MEMS application. They found good agreements between the predicted performances of a fabricated prototype as compared with the experimental measurements. Sisman and Yavuz [14] studied the effect of joule losses on the total efficiency of a thermoelectric generator. They found that the total efficiency of the thermoelectric generator could be greater than that of the conventional DC power generator.

Solar driven thermoelectric generators have recently attracted considerable attention for large scale energy production as a result of improvements in the efficiency of the thermoelectric materials. Chen [15] studied the performance characteristics of solar driven thermoelectric generators, based on a thermodynamic model including four main irreversibilities, which exist usually in solar driven thermoelectric generators. He determined limits of some new performance parameters, such as the efficiency, power output, and load resistance. Recently, Li et al. [16] proposed an experimental prototype concentration solar thermoelectric generator with improved total conversion efficiency. They developed a theoretical model of the concentration solar thermoelectric generator system to predict system performance based on the best available properties of different bulk thermoelectric materials found in the literature, including Bi_2Te_3, skutterudite, and silver antimony lead telluride alloys. They showed that the highest possible efficiency of the concentration solar thermoelectric generator can attain 9.8%, 13.5%, and 14.1% for Bi_2Te_3, skutterudite, and silver antimony lead telluride alloys, respectively.

Consequently, an efficiency analysis of topping cycle consisting of conventional solar concentration power plant with thermoelectric generators placed on the heat collector elements is carried out in the present work. Numerical simulations are carried out for predicting the flow and temperature fields in the working fluid in the thermal system. The overall efficiency ratio due to the thermal systems with and without the presence of the thermoelectric power generators is examined for various operating parameters.

2. Analyses of thermal system with and without presence of topping cycle

Thermal analysis considering the numerical prediction of temperature and flow fields in a tube subjected to a concentrated solar heating in relation to the topping cycle is presented. Since the bulk fluid temperature change in tube is one of the parameters influencing the overall efficiency ratio corresponding with and without thermoelectric elements, the numerical predictions of temperature change in the tube are fruitful. The comparative thermodynamic analyses for the thermal systems with and without thermoelectric generator are given below under the appropriate sub-headings.

2.1. Heat transfer analysis in relation to flow into the tube resembling the topping cycle

The numerical analysis in relation to solar transparent tube resembling the topping cycle is given below.

2.1.1. Governing equations

The steady and compressible flow is considered in the tube. Fluid flow and heat transfer are governed by the equations of conservation of mass momentum and energy. The equation of conservation of mass also known as the continuity equation is:

$$\nabla\cdot\overline{\mathbf{V}} = 0$$

The conservation of momentum equation is:

$$\frac{\partial(\rho\overline{\mathbf{V}})}{\partial t} + \nabla\cdot(\rho\overline{\mathbf{V}}\overline{\mathbf{V}}) = -\nabla\overline{p} + \nabla\cdot\left(\overline{\tau} + \tau^*\right) \tag{1}$$

This Equation is known as the Reynold's Averaged Navier Stokes Equation. $\overline{\tau}$ is the shear stress or viscous stress tensor:

$$\overline{\tau} = 2\mu\mathbf{\Gamma} + \left(\lambda - \frac{2}{3}\mu\right)(\nabla\cdot\overline{\mathbf{V}})\delta_{ij} \tag{2}$$

and τ^* is the 'turbulent stress' or 'Reynold's stress' term and has nine components in a three-dimensional system.

$$\tau^* = -\rho\overline{\mathbf{V}'V'} \tag{3}$$

These additional stresses in the Reynold's Averaged Navier Stokes can be generalized as:

$$\tau^* = \begin{pmatrix} \tau^*_{xx} & \tau^*_{xy} & \tau^*_{xz} \\ \tau^*_{yx} & \tau^*_{yy} & \tau^*_{yz} \\ \tau^*_{xx} & \tau^*_{yz} & \tau^*_{xz} \end{pmatrix} = \begin{pmatrix} -\rho\overline{u'u'} & -\rho\overline{u'v'} & -\rho\overline{u'w'} \\ -\rho\overline{v'u'} & -\rho\overline{v'v'} & -\rho\overline{v'w'} \\ -\rho\overline{w'u'} & -\rho\overline{w'v'} & -\rho\overline{w'w'} \end{pmatrix} \tag{4}$$

The energy equation is given by:

$$\rho C\left(\frac{\partial \overline{T}}{\partial t}+\nabla\cdot(\overline{T}\overline{\mathbf{V}})\right) = -\nabla\cdot\left(\overline{q}+q^{*}\right)+\mu\overline{\Phi} \tag{5}$$

where, $\overline{q}$ is the energy flux:

$$\overline{q} = -k\nabla T \tag{6}$$

and q^{*} is the turbulent energy flux and has three components in a three-dimensional system:

$$q^{*} = \rho C\overline{\mathbf{V}'T'} \tag{7}$$

2.1.2. Standard k–ε model

k–ε turbulence model is used to account for the turbulence effect of the flow in the tube. In order to complete the turbulence model we add a set of equations to solve for turbulent kinetic energy, k and energy dissipation rate ε. Together these equations are known as the k–ε model.

$$\rho\left(\frac{\partial k}{\partial t}+\nabla\cdot k\mathbf{V}\right) = \nabla\cdot\left(\left(\mu+\frac{\mu_t}{\sigma_k}\right)\nabla k\right)+P_k-\rho\varepsilon \tag{8}$$

$$\rho\left(\frac{\partial \varepsilon}{\partial t}+\nabla\cdot\varepsilon\mathbf{V}\right) = \nabla\cdot\left(\left(\mu+\frac{\mu_t}{\sigma_\varepsilon}\right)\nabla\varepsilon\right)+\frac{\varepsilon}{k}(P_k-\rho\varepsilon) \tag{9}$$

where μ_t is the eddy viscosity given by

$$\mu_t = \rho C_\mu\frac{k^2}{\varepsilon} \tag{10}$$

Five empirical constants appear in these equations.

C_μ	C_1	C_2	σ_k	σ_ε
0.09	1.44	1.92	1.00	1.00

2.1.3. Boundary conditions

2.1.3.1. Inlet condition. No slip condition is imposed at the fluid–wall interface.

$$u|_{\text{wall}} = 0$$

The conjugate heat transfer at the boundary is incorporated. This means that temperature of the fluid at the fluid–wall interface is taken to be equal to solid temperature at the wall and the heat conduction normal to the wall in the fluid is taken to be equal to heat conduction normal to the wall in the solid.

$$T_{\text{fluid}}|_{\text{wall}} = T_{\text{solid}}|_{\text{wall}}$$
$$(k(\nabla T)\cdot n)_{\text{fluid}} = (k(\nabla T)\cdot n)_{\text{solid}}$$

where n is the normal vector at the solid–fluid interface.

2.2. Numerical solution

Finite element approach is introduced to solve the governing equations of flow. The details of the numerical scheme are given in COMSOL Multiphysics reference guide [17]. The calculation domain is meshed using the second order Lagrangian elements. The finer grids are located in the area of maximum expected gradients of temperature and velocity; therefore, the grids are finer in the vicinity of the inner pipe while the grids become courser as the distance increases away from the pipe wall. The total number of the elements used in the simulation is 12 064.

2.3. Thermodynamics analysis

2.3.1. Topping cycle with presence of a thermoelectric power generator (TEG)

The thermal efficiency of a solar thermoelectric topping cycle is shown in Fig. 1(a) can be written as

$$\eta_{\text{sys}} = \frac{W_{\text{TE}}+W_{\text{R}}}{Q_s} = \eta_{\text{abs}}[\eta_{\text{R}}+\eta_{\text{TE}}(1-\eta_{\text{R}})] \tag{11}$$

Where $\eta_{\text{abs}} = Q_{\text{H}}/Q_s = 1-(Q_r+Q_c)/Q_s$ is the absorber efficiency, $\eta_{\text{TE}} = W_{\text{TE}}/Q_{\text{H}} = 1-(Q_{\text{L}}/Q_{\text{H}})$ is the thermoelectric generator efficiency and $\eta_R = W_{\text{R}}/Q_{\text{L}}$ is the Rankine cycle efficiency. It should be noted that the term $Q_r + Q_c$ is the loss heat flux from the absorber.

2.3.2. Cycle without thermoelectric power generator (TEG)

The thermal efficiency of an ordinary solar thermal Rankine cycle shown in Fig. 1(b) can be written as

$$\eta'_{\text{sys}} = \eta'_{\text{abs}}\eta'_{\text{R}} \tag{12}$$

where $\eta'_{\text{abs}} = Q'_{\text{H}}/Q'_s$ is the absorber efficiency and $\eta'_{\text{R}} = W'_{\text{R}}/Q'_{\text{H}}$ is the Rankine cycle efficiency.

2.3.3. Overall efficiency ratio of both systems

The overall efficiency ratio of solar thermoelectric topping cycle (Fig. 1(a)) and the efficiency of the ordinary solar thermal Rankine cycle (Fig. 1(b)) is

$$R=\frac{\eta_{\text{sys}}}{\eta'_{\text{sys}}}=\frac{\eta_{\text{abs}}}{\eta'_{\text{abs}}}\left[\frac{\eta_{\text{R}}}{\eta'_{\text{R}}}+\eta_{\text{TE}}\left(\frac{1}{\eta'_{\text{R}}}-\frac{\eta_{\text{R}}}{\eta'_{\text{R}}}\right)\right]\quad R>1\ \text{is required} \tag{13}$$

$R > 1$ indicates an improvement of efficiency in using thermoelectric power generator in the solar thermal Rankine cycle i.e. $\eta_{\text{sys}} > \eta'_{\text{sys}}$ that means $(\eta_{\text{withTE}})_{\text{sys}} > (\eta_{\text{withoutTE}})_{\text{sys}}$. Figs. 2 and 3 shows the region for $(\eta_{\text{withTE}})_{\text{sys}} > (\eta_{\text{withoutTE}})_{\text{sys}}$ i.e. $R > 1$ for constant thermoelectric efficiency assumed.

In order to compare the thermal efficiency of the cycles with and without the presence of thermoelectric generator, two cases are introduced below:

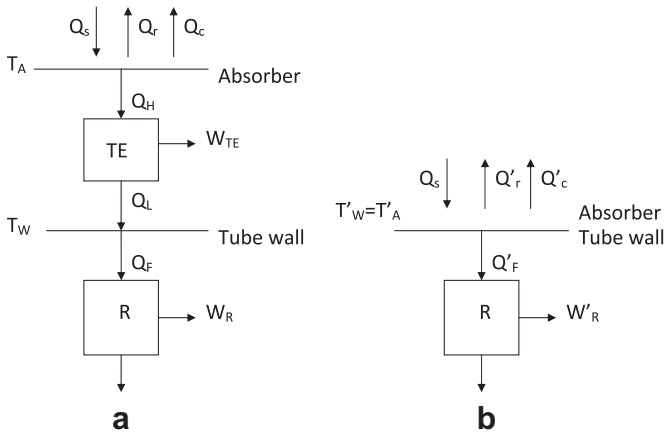

Fig. 1. (a) Schematic of solar thermoelectric topping cycle and (b) Solar thermal Rankine cycle.

2.4. Case a: the solar thermoelectric topping cycle

The energy balance across the absorber for the solar thermoelectric topping cycle (Fig. 1(a)) yields:

$$Q_S = Q_H + Q_r + Q_c \tag{14}$$

On the other hand, the efficiency of the thermoelectric generator is given by

$$\eta_{TE} = 1 - \frac{Q_F}{Q_H}$$

.

Therefore, equation (14) becomes:

$$Q_S = \frac{Q_F}{1-\eta_{TE}} + Q_r + Q_c \tag{15}$$

Let us consider the thermoelectric generator operates at conditions resulting in the maximum thermal efficiency. Thus, the maximum efficiency can be written as [18]:

$$\eta_{TE} = (1-\theta)\frac{\sqrt{1+ZT_{ave}}-1}{\sqrt{1+ZT_{ave}}-\theta}$$

Where $\theta = T_W/T_A$.

On the other hand

$$Q_F = Q_L = \left(\frac{1}{\eta_{TE}} - 1\right) W_{TE} \tag{16}$$

The power generated by the thermoelectric generator W_{TE} when operates at its maximum efficiency is [18]:

$$W_{TE} = KT_W \frac{2(1-\theta)^2 ZT_{ave}\sqrt{1+ZT_{ave}}}{\theta(1+\theta)\left(1+\sqrt{1+ZT_{ave}}\right)^2}$$

However, the radiation heat loss from the absorber surface is:

$$Q_r = \sigma \in \left(T_A^4 - T_{sky}^4\right) \tag{17}$$

where T_{sky} is defined as $T_{sky} = T_{amb} - 8$ (K) and T_{amb} is the ambient temperature [19].

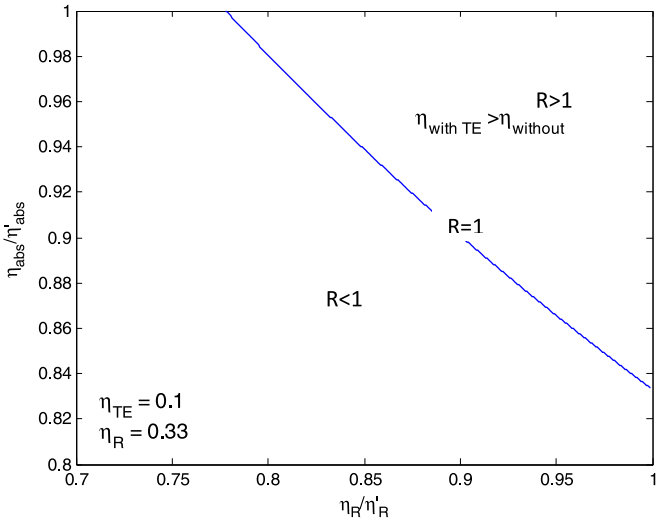

Fig. 2. Region of possible efficiency improvement in a topping cycle with 10% thermoelectric efficiency and 33% Rankine cycle efficiency.

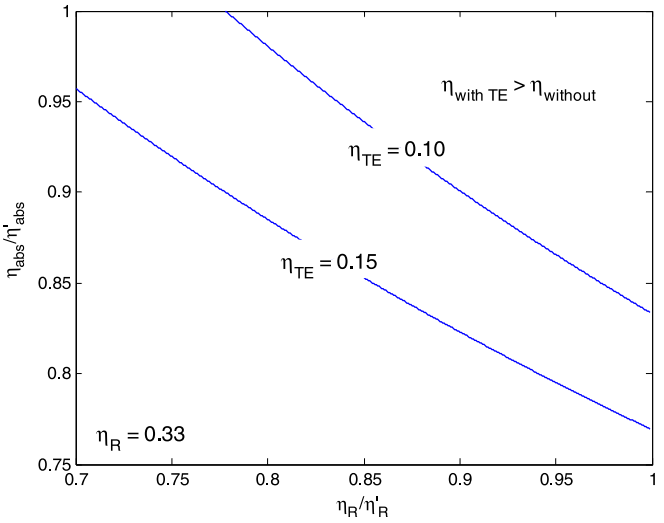

Fig. 3. Regions of possible efficiency improvement of a topping cycle for thermoelectric generator efficiencies of 10% and 15%.

The convection heat loss to the surroundings from the absorber is:

$$Q_c = h_o(T_A - T_{amb}) \tag{18}$$

where h_o is the absorber outer surface heat transfer coefficient.

Substituting equations (17) and (18) in equation (15) and solving equations (15) and (16) for temperature T_A and T_W yields the prediction of absorber and tube wall temperatures, T_A and T_W. Since equations (15) and (16) are non-linear, a numerical solution is required.

2.5. Case b: the solar thermal Rankine cycle with absence of thermoelectric element

The energy balance for the solar thermal Rankine cycle (Fig. 1(b)) is

$$Q_S = Q'_F + Q'_r + Q'_c \tag{19}$$

where

$$Q'_F = h_i(T'_A - T_F) \tag{20}$$

where h_i is the heat transfer coefficient at inner surface of the pipe used in the system.

Equation (19) can be solved with combining equations (17), (18), and (20). It should be noted that the values of absorber temperatures in equations (17) and (18) are different in solar thermoelectric topping cycle and in the solar thermal Rankine cycle. In equations (16)–(20), the lump thermodynamic analysis is considered and the influence temporal variation including daily and yearly variation of solar thermal irradiance on the solar thermoelectric topping and solar thermal Rankine cycles are neglected. This provides the comparison of the thermal efficiency of both cycles on the average data values.

3. Results and discussion

The efficiency of the topping cycle including the thermoelectric module (power generator) is analyzed. The topping cycle efficiency is compared with its counterpart without the presence of the thermoelectric power generator operating under the same heat source and heat sink conditions (Table 1).

Fig. 2 shows the ratio of absorber efficiency ratio (η_{abs}/η'_{abs}) with the Rankine cycle efficiency ratio (η_R/η'_R) for different overall

Table 1
Parameters used in the analysis.

Parameter	Base value
Solar radiation (insolation), q_s (W/m^2) (concentration ratio: 68 suns)	68000
Absorber emissivity [20]	0.15
Outer heat transfer coefficient, h_o (W/m^2 K)	10
Tube inner heat transfer coefficient, h_i (W/m^2 K)	500
Tube inner heat transfer fluid bulk temperature, T_F (K)	450
Surrounding ambient temperature, T_{amb} (K)	300
Effective sky temperature, T_{sky} (K) = T_{amb} − 8 [19]	292
The Figure of Merit, Z (1/K)	0.003
The thermal conductivity, K (W/K) [20] ($K = kA/L$ for unit area $A = 1$, $K = k/L = 1.5/0.003 = 500$ W/K)	500

efficiency ratio (R, equation (13)) for the cycle with and without the presence of the thermoelectric power generator. The region where R is greater than 1 ($R > 1$) represents the overall topping cycle efficiency with the presence of the thermoelectric power generator is greater than that of without the thermoelectric power generator. It is evident that $R > 1$ is limited to a small region in the figure where the absorber and the Rankine efficiency ratios are both above 90%. This situation is true for the thermoelectric generator efficiency of 10%. In the case of high efficiency (15%) of the thermoelectric generator, the region in the figure becomes slightly larger than that corresponding to 10% thermoelectric generator efficiency, which is shown in Fig. 3. This is attributed to the improvement in the overall efficiency of the thermal system incorporating the thermoelectric generator because of the improvement of the thermoelectric generator efficiency (equation (11)). However, the region for $R > 1$ is not substantial increased due to the fact that the absorber efficiency and the Rankine efficiency of the topping cycle with the presence of the thermoelectric power generator do not improve considerably as observed from Fig. 3.

In order to examine the influence of operating parameters on the overall efficiency ratio (R), Figs. 4–8 are plotted. The absorption and emission of the collector surface is assumed to be independent of the amount of solar radiation in line with the previous work [19]. In Fig. 4, the overall efficiency ratio variation with the solar radiation input (q_s) is shown. The overall efficiency ratio reduces almost linearly with increasing solar radiation. This indicates that increasing solar radiation improves the overall efficiency of the thermal system. However, the thermal losses associated with the thermal system with the presence of thermoelectric generator

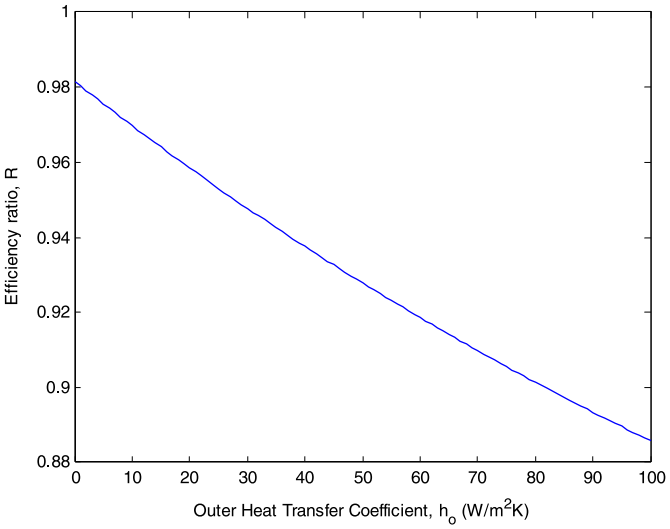

Fig. 5. Variation of the overall efficiency ratio with the outer heat transfer coefficient.

increases with increasing solar radiation. Therefore, the overall efficiency of the system with the presence of thermoelectric generator becomes less than that corresponding to the thermal system without thermoelectric generator. This is more pronounced with increasing solar radiation. Consequently, the overall efficiency ratio reduces with increasing solar radiation. It should be noted that the reduction in the overall efficiency ratio is not significant (~2%) despite the fact that increase in solar radiation is almost 10 times of the minimum value used in the simulations.

Figs. 5 and 6 show the overall efficiency ratio (R) with the heat transfer coefficient at the outer and inner surface of the tube, respectively. It should be noted that the outer surface of the tube is extended to include the absorber outer surface. Increasing the outer heat transfer coefficient reduces the overall efficiency ratio (Fig. 5). In this case, convective heat loss from the absorber surface reduces the overall efficiency of the both thermal systems. However, the reduction of the overall efficiency of the thermal system with the presence of the thermoelectric generator is higher than that of the system without thermoelectric generator. Consequently, the overall efficiency of the thermal system with the presence of the thermoelectric generator is more sensitive for the convection heat

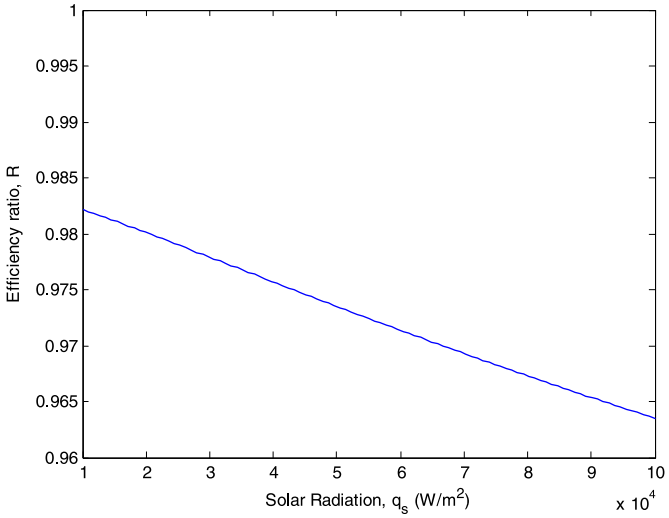

Fig. 4. Variation of the overall efficiency ratio with concentrated solar radiation over the heat collection element (the receiver tube).

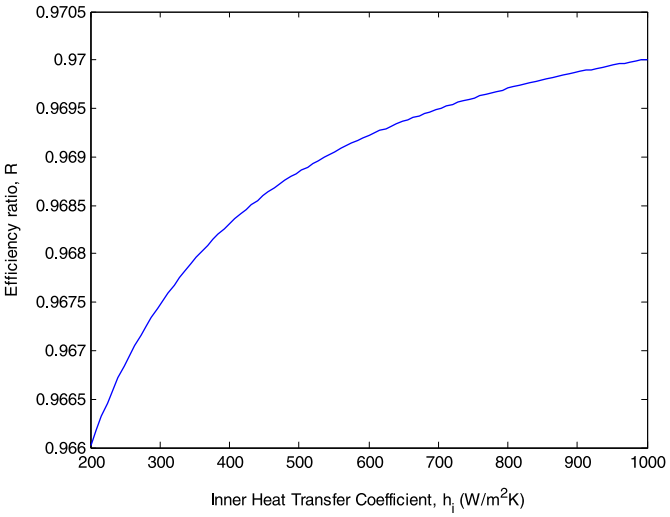

Fig. 6. Variation of the overall efficiency ratio with the inner tube heat transfer coefficient.

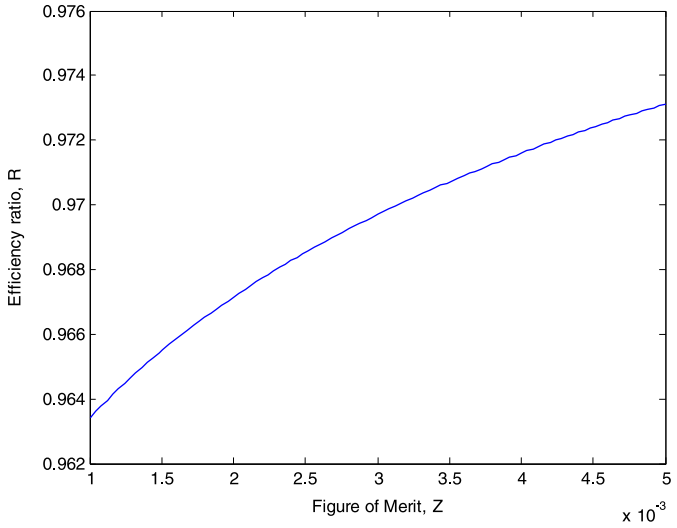

Fig. 7. Variation of the overall efficiency ratio with the figure of merit of the thermoelectric generator.

loss from the absorber surface than its counterpart without the thermoelectric generator. In the case of Fig. 6, the overall efficiency ratio improves with increasing tube inner wall heat transfer coefficient. This reveals that the improvement in the overall efficiency of the thermal system with the presence of the thermoelectric generator is more than that of the thermal system without thermoelectric power generator. This is more pronounced as the inner wall heat transfer coefficient increases from 300 to 500 W/m^2 K. The amount of increase in the efficiency ratio is in the order of 1.27×10^{-3} for the large range of the heat transfer coefficients, 100–1000 W/m^2 K. However, increase in the overall efficiency ratio almost saturates towards the outer limit of the heat transfer coefficient ($h_i > 900$ W/m^2 K) used in the simulations. Consequently, further increase in the heat transfer coefficient results in negligible increase in the overall efficiency ratio.

Fig. 7 shows the overall efficiency ratio with the Figure of Merit. The overall efficiency ratio increases with increasing the Figure of Merit. This is associated with the increase of the thermoelectric generator efficiency, which adds to the enhancement of the overall efficiency of the thermal system with the presence of the thermoelectric generator. The increase in the overall efficiency ratio is ~1% for the range of the Figure of Merit from 10^{-3} to 5×10^{-3}. It should be noted that increasing the Figure of Merit is costly due to cost of the high efficiency thermoelectric generator, despite the fact that the improvement in the overall efficiency ratio is considerably small.

Although thermodynamic analysis gives insight into parameters influencing the overall efficiency ratio, temperature variation along the tube is important to examine the influence of bulk fluid temperature on the overall efficiency ratio. The range of the fluid bulk temperature depends on temperature change in the tube with and without presence of the thermoelectric element. Therefore, numerical simulation enables to predict temperature change per unit metre of a tube. Fig. 8 shows temperature variation along the symmetry axis of the tube as predicted from the simulations. It is evident that temperature distribution inside the tube is influenced by the presence of thermoelectric generator located outside of the tube. In this case, the thermoelectric generators contributed to the thermal resistance outside of the tube while reducing the tube inner wall temperature. Consequently, temperature rise in the working fluid becomes less for thermal system with the presence of the thermoelectric generator as compared to that of without thermoelectric generator. In addition, a high vacuum sealing at the outer surface of the tube reduces the heat transfer losses from the tube surface. In this case, working fluid temperature increases towards the tube exit. Fig. 9 shows overall efficiency ratio with working fluid bulk temperature. The overall efficiency ratio increases to reach maximum at working fluid temperature of about 400 K. However, increasing fluid temperature further reduces the overall efficiency ratio. This is associated with the followings: i) increasing fluid temperature enhances the overall efficiency of the thermal system without thermoelectric generator as observed from Fig. 8, and ii) overall efficiency of the thermal system with thermoelectric generator does not increase as much as its counterpart without thermoelectric generator because of the thermal losses due to the presence of thermoelectric generator. Consequently, operating the thermal system with the presence of the thermoelectric generator at certain temperature range has advantage of obtaining the improved overall efficiency ratio.

Finally, Fig. 10 shows the comparison of the model used with experimental data in order to verify the accuracy of the model. The experimental data is obtained from tests conducted from June 1992 through January 1993 on the AZTRAK rotating test platform at Sandia National Laboratories. The trough on the rotating test platform consists of an LS-2 type collector segment with two Luz Cermet heat collector elements of 4.06 m each and a concentration

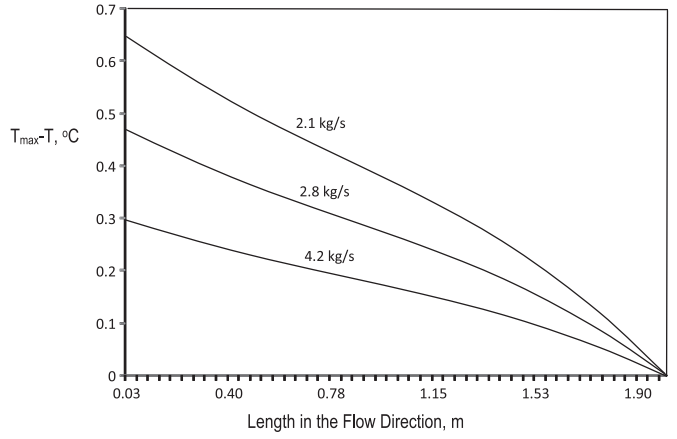

Fig. 8. Temperature variation along the symmetry axis of the tube.

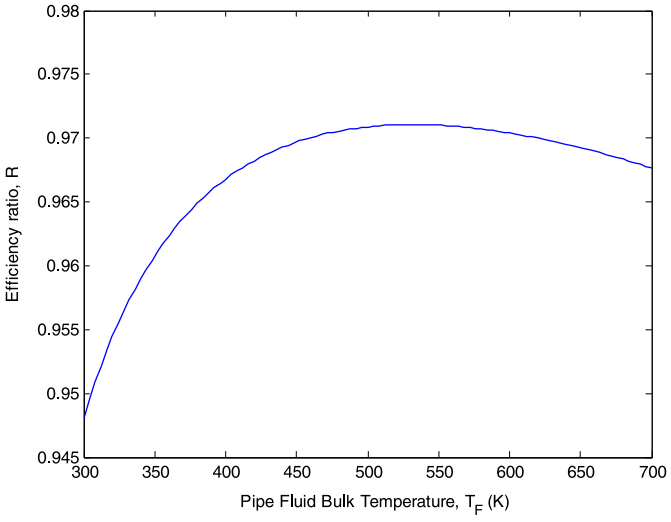

Fig. 9. Variation of the overall efficiency ratio with the pipe fluid bulk temperature.

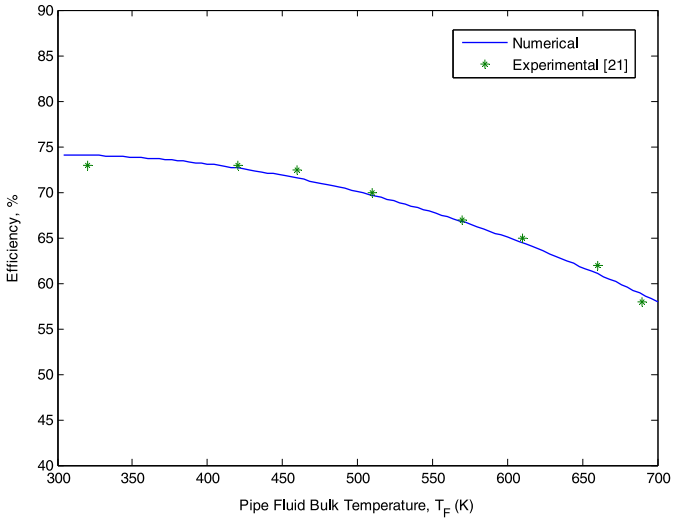

Fig. 10. Comparison of numerical model with experimental data (LS-2 Collector, Syltherm 800, Luz Cermet Selective Coating, Solar (NIP) ~ 800–970 W/m^2) [21].

ratio of 71. All the data used in the comparison and a detailed explanation of the AZTRAK rotating test platform tests can be found in Ref. [21]. The efficiency of the solar energy transfer decreases as the bulk fluid temperature increases. This is attributed to the increase of heat losses to the ambient as a result of increase in the bulk fluid temperature.

4. Conclusion

Efficiency analysis of topping cycle is carried out and overall efficiency ratio due to the thermal systems with and without the presence of the thermoelectric power generator is examined for various operating parameters. The numerical simulations for predicting the flow and temperature fields in the working fluid in the thermal system are carried out. The overall efficiency ratio is introduced to assess the performance of the thermal system with the presence of the thermoelectric generator in reference to its counterpart without thermoelectric generator. It is found that overall efficiency ratio can be higher than 1.0 for certain range of the absorber and the Rankine efficiency ratios. However, the improvement in the overall efficiency ratio requires the high ratios of the absorber and the Rankine efficiencies. This is more pronounced when the thermoelectric generator efficiency reduces to 10%. Increasing the solar radiation and outer surface heat transfer coefficient reduces the overall efficiency ratio due to the losses associated in the thermal system. In this case, the overall efficiency of the thermal system without thermal electric generator increases more than that corresponding to the thermal system with the presence of the thermoelectric generator. The increase in tube inner wall heat transfer coefficient and the Figure of Merit enhance the overall efficiency ratio. However, the increase in the overall efficiency ratio is not significant. The small increase in the overall ratio with large increase in the Figure of Merit is associated with the low efficiency of the thermoelectric generator. The overall efficiency ratio increases to reach its maximum with increasing working fluid temperature, provided that working fluid temperature beyond 400 K lowers the overall efficiency ratio.

Acknowledgement

The authors acknowledge the support of Center of Excellence for Scientific Research Collaboration with MIT and King Fahd University of Petroleum and Minerals, Dhahran, Saudi Arabia, for this work.

References

[1] Amatya R, Ram RJ. Solar thermoelectric generator for micropower applications. Journal of Electronic Materials 2010;39:1735–40.
[2] Kassas M. Thermodynamic analysis of a thermoelectric device. International Journal of Exergy 2007;4(2):168–79.
[3] Yamashita O. Effect of linear temperature dependence of thermoelectric properties on energy conversion efficiency. Energy Conversion and Management 2008;49:3163–9.
[4] Yilbas BS, Sahin AZ. Thermoelectric device and optimum external load parameter and slenderness ratio. Energy 2010;35:5380–4.
[5] Hsiao YY, Chang WC, Chen SL. A mathematic model of thermoelectric module with applications on waste heat recovery from automobile engine. Energy 2010;35:1447–54.
[6] Champier D, Bedecarrats JP, Rivaletto M, Strub F. Thermoelectric power generation from biomass cook stoves. Energy 2010;35:935–42.
[7] Kubo M, Shinoda M, Furuhata T, Kitagawa K. Optimization of the incision size and cold-end temperature of a thermoelectric device. Energy 2005;30:2156–70.
[8] Gou X, Xiao H, Yang S. Modeling, experimental study and optimization on low-temperature waste heat thermoelectric generator system. Applied Energy 2010;87:3131–6.
[9] Omer SA, Infield DG. Design optimization of thermoelectric devices for solar power generation. Solar Energy Materials and Solar Cells 1998;53:67–82.
[10] Astrain D, Vian JG, Dominguez M. Increase of COP in the thermoelectric refrigeration by the optimization of heat dissipation. Applied Thermal Engineering 2003;23:2183–200.
[11] Khattab NM, El Shenawy ET. Optimal operation of thermoelectric cooler driven by solar thermoelectric generator. Energy Conversion and Management 2006;47:407–26.
[12] Abdul-Wahab SA, Elkamel A, Al-Damkhi AM, Al-Habsi IA, Al-Rubai'ey' HS, Al-Battashi AK, et al. Design and experimental investigation of portable solar thermoelectric refrigerator. Renewable Energy 2009;34:30–4.
[13] Hwang GS, Gross AJ, Kim H, Lee SW, Ghafouri N, Huang BL, et al. Micro thermoelectric cooler: planar multistage. International Journal of Heat and Mass Transfer 2009;52:1843–52.
[14] Sisman A, Yavuz H. The effect of joule losses on the total efficiency of a thermoelectric power cycle. Energy 1995;20:573–6.
[15] Chen J. Thermodynamic analysis of a solar-driven thermoelectric generator. Journal of Applied Physics 1996;79:2717–21.
[16] Li P, Cai L, Zhai P, Tang X, Zhang Q, Niino M. Design of concentration solar thermoelectric generator. Journal of Electronic Materials 2010;39:1522–30.
[17] math.nju.edu.cn/help/mathhpc/doc/comsol/command.pdf.
[18] Sahin AZ, Yilbas BS. Improving thermal efficiency of solar thermal power plants by using thermoelectric generators. In: Engineering congress on alternative energy applications: option or necessity? Kuwait, November 2–6, 2009.
[19] Forristall R. Heat transfer analysis and modeling of a parabolic trough solar receiver implemented in engineering equation solver. National Renewable Energy Laboratory; October 2003. NREL/TP-550–34169.
[20] Cheng YH, Lin WK. Geometric optimization of thermoelectric coolers in a confined volume using genetic algorithms. Applied Thermal Engineering 2005;25:2983–97.
[21] Dudley VE, Kolb GJ, Sloan M, Kearney D. Test results: SEGS LS-2 solar collector. Albuquerque, NM: SANDIA National Laboratories; December 1994. SAND94–1884.

Nomenclature

K: overall thermal conductivity of the thermoelectric generator, W/K
Q: heat flux, W
R: overall efficiency ratio (Equation (3))
T: temperature, K
W: power output, W
Z: figure of merit, 1/K
ε: emissivity
η: efficiency
θ: dimensionless temperature $= T_W/T_A$
σ: Stefan–Boltzmann constant

Subscripts
A: absorber
abs: absorber
amb: ambient
ave: average
c: convection
F: fluid
H: high temperature reservoir
i: inner
L: low temperature reservoir
r: radiation
R: Rankine
o: outer
s: solar
sky: sky
sys: system
TE: thermoelectric
W: wall